Hydrological Processes

WILEY

RESEARCH ARTICLE OPEN ACCESS

The Role of Snowmelt on the Recharge Dynamics of a Vadose Alpine Karst

Eva Kaminsky[1,2] | Barbara Funk[1,3] | Adrian Flores-Orozco[3] | Lukas Plan[1]

[1]Karst and Cave Group, Geological Paleontological Department, Natural History Museum, Vienna, Austria | [2]Institute of Soil Physics and Rural Water Management, Department of Landscape, Water and Infrastructure, BOKU University, Vienna, Austria | [3]Research Unit of Geophysics, Department of Geodesy and Geoinformation, TU Wien, Vienna, Austria

Correspondence: Eva Kaminsky (eva.kaminsky@nhm.at)

Received: 31 January 2025 | **Revised:** 13 June 2025 | **Accepted:** 8 July 2025

Funding: This work was supported by the Austrian Science Fund (FWF): P36065-N. E.K. thanks the support of the Hochschuljubiläumsfonds of the City of Vienna: H-912466/2022. B.F. thanks the support of the Hochschuljubiläumsfonds of the City of Vienna: H-876947/2022.

Keywords: cave drip water | ERT | karst | recharge processes | snowmelt | vadose zone

ABSTRACT

In Alpine karst aquifers, snowmelt plays a crucial role in groundwater recharge, yet the processes governing water flow through the soil and epikarst into the vadose zone and to the phreatic zone remain poorly understood. This study aims at shedding some light on paths and mechanisms for infiltration, flow, and accumulation of snowmelt in comparison to rainwater in karstic systems. In particular, we present results for the upper vadose zone of the Hochschwab karst massif (Eastern Alps, Austria), a crucial water source for the capital of Vienna. We combined geophysical and hydrological methods to distinguish different infiltration processes. Data were collected at a cave (1896 m above sea level) over 3 weeks in March and April 2024, during which 12 infiltration events were observed—nine through diurnal cycles of snowmelt and three mixed with effective rain. Additionally, dry and wet conditions in the following summer were monitored to provide a seasonal comparison of infiltration dynamics. Monitoring included cave drip water at a V-notch weir (discharge, electrical conductivity, and temperature), soil moisture measurements at depths of 5–30 cm, and electrical resistivity tomography (ERT), utilising 96 electrodes between the cave ceiling and the surface. Measurements at the weir in the cave indicate higher flow rates during heavy precipitation than during snowmelt, while the ERT images show the highest saturation during snowmelt, especially in the bedrock. Hence, results show that snowmelt primarily leads to diffuse recharge, with an overall increase in the saturation of the epikarst and rock, while rain events demonstrate a quick recharge pattern. These findings emphasise the importance of snowmelt as a diffuse recharge source contributing to water storage and underline that the integration of multiple sensors is crucial for understanding the variability of recharge processes in Alpine karst systems under different meteorological conditions.

1 | Introduction

Karst aquifers are of great importance for drinking water supply worldwide (Goldscheider et al. 2020; Stevanović 2019), yet developing accurate hydrogeological models to predict their response to changes in meteorological conditions is challenging due to their dual porosity. While water flow through large fissures and fractures represents the rapid flow (e.g., Ford and Williams 2007; Hartmann et al. 2021), slow percolation of water through the matrix enlarges the residence time of water in karst systems and enhances the time for natural purification (Einsiedl et al. 2009; Reberski et al. 2022). Data from karst springs is often used to quantify the dual porosity flow by applying hydrological models. Different zones of karst aquifers (i.e., the soil cover and epikarst, the vadose zone, and the phreatic zone) have different physical characteristics (e.g., De Waele and Gutiérrez 2022; Ford

and Williams 2007) and up to date, the actual parameters controlling the water flow in karst aquifers are still poorly understood and highly dependent on the regional karst system (e.g., Hartmann et al. 2014).

The soil and epikarst (uppermost weathered zone of the bedrock) can vary significantly from region to region and its development is decisive for water flow in the karst system (Hartmann et al. 2021; Klimchouk 2004; Williams 2008). Understanding the relationship between epikarst and soil is crucial for water flow and storage (Meeks and Hunkeler 2015). Speleological investigations provide direct observations in the vadose zone and caves with dripping water can act as a large natural lysimeter. Some studies analysed cave dripping water for the characterisation of the upper vadose zone, where storage potential (Liu et al. 2016; Meeks and Hunkeler 2015; Perrin et al. 2003; Poulain et al. 2018) as well as quick responses (< 10 min) to rain events were observed (Kaminsky et al. 2021). Thus, the soil and/or epikarst has a high potential for water storage (Arbel et al. 2010; Meeks and Hunkeler 2015; Trček et al. 2006; Williams 2008) and the storage capacity could be more significant than storage in the underlying phreatic zone (Perrin et al. 2003; Klimchouk 2004). Hence, the development and origin of the epikarst are of crucial importance, and attributes a high porosity, permeability and storage capacity to a soil-covered mature epikarst.

To study the epikarst, hydrographic or hydrochemical monitoring in the upper vadose zone, for example, of drip water in caves in combination with pedological monitoring, such as soil moisture, is often a valuable source of information (Berthelin et al. 2023; Ries et al. 2015). However, due to the strong heterogeneity of karst areas, other methods with a higher spatial resolution are necessary to fully capture the variations of water storage in the upper vadose zone.

Geophysical techniques can provide quasi-continuous information about the properties of the subsurface, permitting the delineation of structures with higher spatial resolution than "point-scale" investigations such as hydrological measurements or the analysis of soil and water samples (e.g., Binley et al. 2015; Şener et al. 2021). The electric resistivity tomography (ERT) provides information about the electrical resistivity of the subsurface, which is controlled by the porosity, the saturation, the water (fluid) electrical conductivity (σw) and the interfacial conductivity, which takes place at the grain-water interface (e.g., Slater et al. 2006). Monitoring applications, where changes in porosity, fluid and interfacial conductivity can be neglected, permit determining the temporal evolution of the water saturation in a study area (Kemna et al. 2002; Perera-Burgos et al. 2024; Zhang et al. 2024). Several studies used ERT monitoring to characterise water infiltration in karstic systems (Carriere et al. 2015; Carrière and Chalikakis 2022; Houser et al. 2016; Watlet et al. 2018) and water flow in cave conduits (Martel et al. 2018; Robert et al. 2012). Watlet et al. (2018) reported an increased resistivity in spring and summer and a decrease in resistivity, associated with groundwater recharge of the vadose zone, in winter at the Rochefort Cave Laboratory (Belgium). However, to the best of our knowledge, the investigation with geophysical methods of water recharge due to snowmelt has not been addressed to date in high Alpine karst. In Alpine karst aquifers, the snowmelt water recharge is critical for the total annual discharge and occurs mainly in spring (Brussolo et al. 2022; Lorenzi et al. 2022; Plan et al. 2010; Tague and Grant 2009). Hence, the water flow and storage due to different recharge processes, especially snowmelt, have often been studied at springs (e.g., Cochand et al. 2019; Fan et al. 2023; Reisch and Toran 2014; Zeydalinejad et al. 2024), but rarely in-depth for the epikarst. Two studies in pre-Alpine karst revealed contradictory results. Meeks and Hunkeler (2015) found that prolonged periods of snowmelt promote perched storage in surficial soils and encourage surficial, lateral flow to preferential flow paths, whereas Eeckman et al. (2024) found that snowmelt infiltrates hardly below 30 cm depth. Inconsistencies in various studies indicate that the infiltration mechanisms within the epikarst are highly dependent on the study site and need to be further assessed. The integration of hydrological, pedological and ERT monitoring allows a common interpretation of the infiltration processes in the epikarst through a different spatial resolution.

The objectives of our investigations are (1) to understand the flow dynamics of snowmelt infiltration, namely the partitioning between water storage and flow; and (2) to investigate the changes in storage and discharge characteristics during different phases of the hydrological cycle, including snowmelt, dry periods, and after precipitation. Therefore, we present monitoring results for the infiltration of snowmelt (over 3 weeks). In addition, summer monitoring was carried out under dry and wet conditions for comparison. A high-resolution multi-sensor approach was chosen in order to best capture the complexity of the karst system. The study was carried out in a cave located in an Alpine, karstic environment at an altitude of 1896 m above sea level (a.s.l.) in Austria.

2 | Materials and Methods

2.1 | Study Area

The Hochschwab massif, 80 km southwest of Vienna in the Austrian state of Styria, is one of the extensive karst plateaus of the Northern Calcareous Alps (Plan 2016) with an area of 650 km^2 and the peak at 2277 m a.s.l. It represents the most important aquifer for Vienna's water supply. The climate is Alpine with annual average temperatures of 1.9°C, a sum of 2376 mm annual and 556 mm winter precipitation, and 58 days of snowstorm at the cave (1896 m a.s.l., reference period 1971 to 2000 after Land Steiermark 2024). The snowpack at the catchment is affected by wind, similar to the wind at Eismauer (Figure 1), leading to a wind-packed snow cover with spatial differences. The wind transports the snow mainly in hollows and dolines, where the wind-packed snow can remain until late spring. The south-facing slope causes the remaining snow to melt quickly. As a result, the snow cover in the catchment area varies strongly spatially, with intermittent snowpacks at many locations and persistent snow cover in areas where wind drifts occur. Long-term observations based on cave research over the last 20 years have never shown a continuous snow cover of more than 10 cm.

Due to its high importance for water supply, the Hochschwab became an intensely studied karst massif during the last decades (e.g., Exel 2014; Kaminsky et al. 2021; Kuschnig 2001; Plan et al. 2009). The geology of the Hochschwab is dominated

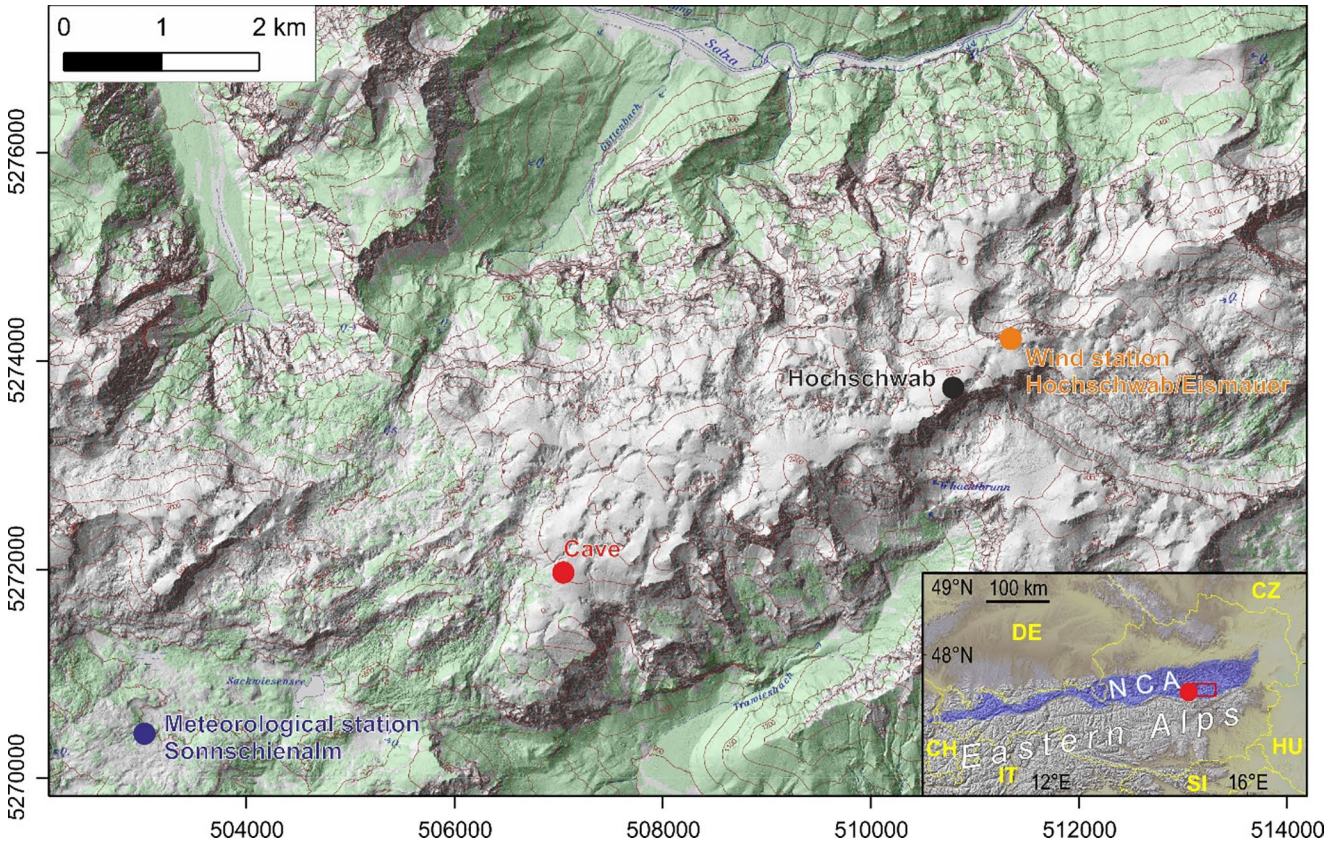

FIGURE 1 | Position of the study area in the Alpine region of the Hochschwab plateau with the cave and meteorological stations (Coordinates: UTM 33N).

by Triassic carbonate rocks and the most common lithologies are limestone and dolomite of Wetterstein formation reaching up to 1.5 km in thickness (Bryda et al. 2013). The present-day landscape has been profoundly shaped by a complex multi-phase tectonic evolution, karstification, and the Pleistocene glaciations (Bauer et al. 2016; Bryda et al. 2013; Mandl 2000; Plan and Decker 2006). Plan et al. (2009) have shown that re-juvenation of the karst surface due to glacial erosion influences the infiltration and storage of water and vulnerable zones are delineated. In glacial cirques and similar areas, the surface is less than 20 ka old and the lack of a soil and epikarst layer leads to marginal storage (Kaminsky et al. 2021). In contrast, where palaeo-landscapes have been preserved on elevated sites that have emerged from the ice cover, such as modern Nunataker, a much thicker soil and epikarst layer allows for storage and less rapid infiltration (Exel et al. 2016; Plan and Decker 2006; Zemann 2024).

The 5.5 km long cave is an at least 5 Ma old karst cave formed under phreatic conditions. It was uplifted 1.3 km above the present base level and was intersected by the surface of a palaeo-landscape. This cave was chosen as a study site because the sub-horizontal cave passages near the entrance (Figure 2) offer the possibility of investigating changes in water saturation in the soil, epikarst, and upper vadose zone using ERT monitoring. Inside the cave, drip water has already been monitored for several years. The palaeo landscape is less overprinted by glacial erosion, resulting in a soil cover with a thickness of up to 40 cm. The cave opens at 1896 m a.s.l. (Figure 1) above the tree line in Dachstein limestone and dolomite. For the first 50 m, the cave passages extend sub-horizontally into the mountain, while the surface above the cave rises with a slope of around 35%, resulting in a rock overburden of up to 28 m (Figure 2). The palaeo surface contains a soil cover with a well-developed epikarst layer followed by the bedrock of the vadose zone. A detailed geological and pedological description of the cave and its surrounding area is provided by Djukic et al. (2010), Exel et al. (2016), Plan et al. (2019), and Zemann (2024).

2.2 | Field Setup, Data Source and Processing

2.2.1 | Measurements Outside the Cave

A meteorological station has been installed above the entrance to a cave (Figure 2c) to measure precipitation (P) and temperature (T) at 5-min intervals. P is measured by a tipping bucket rain gauge. Thermometers measure the air and ground T at a depth of 3 cm using one sensor in the gravel and one sensor in the soil. Additionally, soil T was measured along with the volumetric water content (HOBO Pendant Logger, resolution ±0.04°C). Snow depth (ultrasound measurement) was provided by MA31 Wiener Wasser from the meteorological station "Hochschwab Sonnschienalm" at 1524 m a.s.l. and 4 km SW from the study site. The wind speed data for the Hochschwab/Eismauer location are provided by GeoSphere Austria (Figure 1). The slope above the cave is exposed to the predominant wind from the

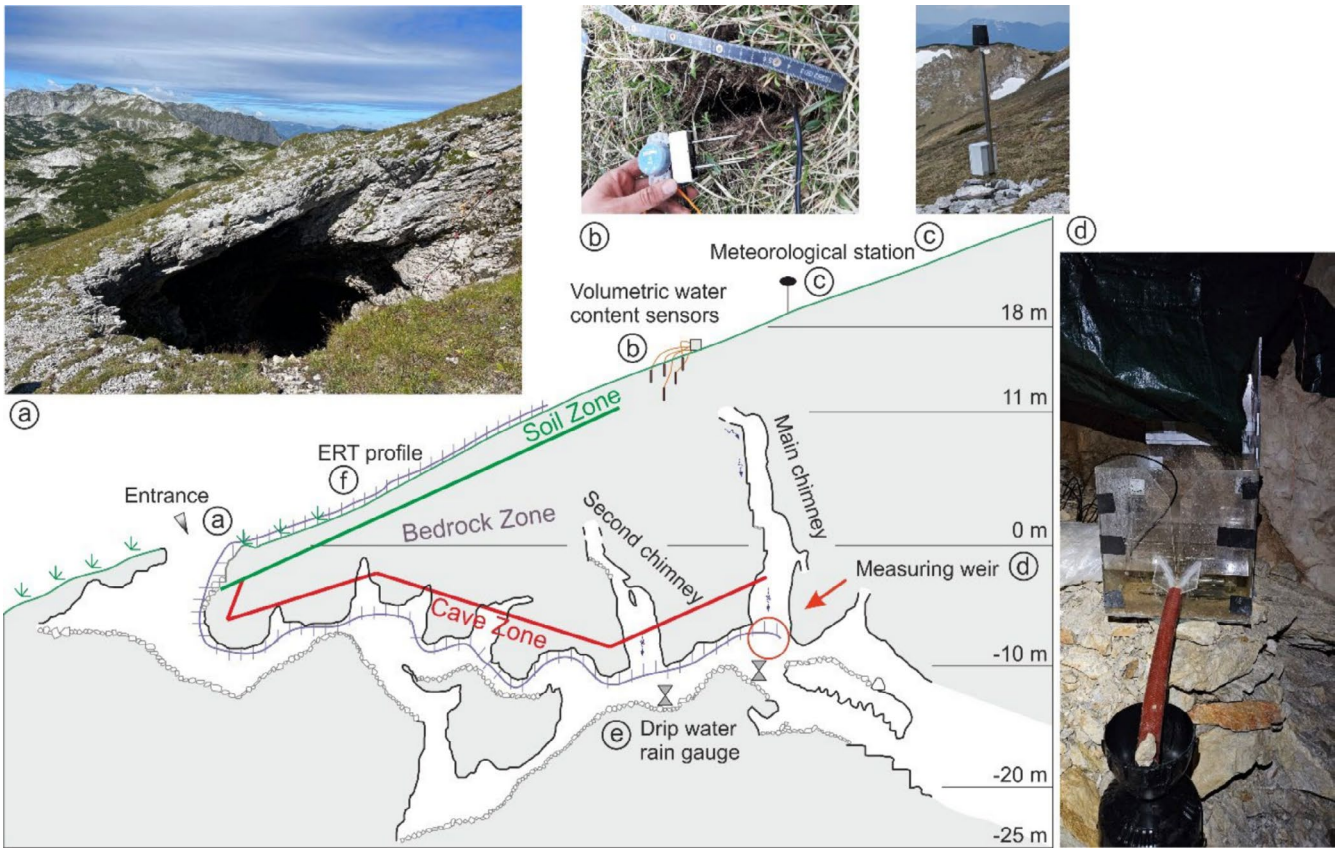

FIGURE 2 | Schematic section of the area near the entrance to the cave with all sensors including photographs: (a) the doline cave entrance with a diameter of 9 m; (b) six volumetric water content sensors that were placed in the soil; (c) rain gauge (measures liquid precipitation); (d) measuring weir; (e) a second rain gauge measures drip water in a second chimney; and (f) a polygon symbolises the ERT electrodes.

west, increasing the uncertainties in the meteorological data. A simple approach from Oudin et al. (2005) was used to compute potential evapotranspiration (ETp). It considers air temperature and global radiation and has already been successfully applied by Wagner et al. (2013) and Kaminsky et al. (2021) in a karst catchment. Effective precipitation is defined as > 2 mm during the snowmelt monitoring (P-ETp).

Volumetric water content (VWC) is measured at three locations above the chimney in the cave (Figure 2), using five TEROS 10 (measures only VWC) plus separate T sensors and one TEROS 12 sensor (Figure 2b; accuracy with generic calibration ±0.03 m^3/m^3). TEROS 10 was buried at location 1 at 20 cm depth, location 2 at 5, 20, and 30 cm depth, and location 3 at 5 cm depth (locations are shown in the Figure S1). At location 3, TEROS 12, which measures T and electrical conductivity (EC) in addition to VWC, was buried at 20 cm. The upper soil sensors (in 5 and 20 cm depth) can be attributed to the soil profile 1 from Exel (2014) which is mainly characterised by clay and silt with a high humus content and slightly acid pH (5–6.6). Only at location 1 can the sensor at 20 cm be attributed to soil profile 2 from Exel (2014) with an alkaline sandy-silty soil. The third sensor at location 3 (35 cm depth) was installed close to the soil-rock interface where gravel occurred. Further details on the soil characteristics and profiles from sensor installation can be found in Exel (2014) and Zemann (2024). Wet and dry conditions are defined as the minimum and maximum of the VWC at each sensor.

2.2.2 | Measurements Inside the Cave

Drip water from a chimney with 7 m of overburden at its narrow top is collected with a plastic sheet and channelled into an acrylic glass box, with a v-shaped notch acting as a Thompson weir (Exel 2014, Figure 2d). Pressure head, T, and EC are monitored in a 5-min interval with a multiparameter pressure rod (KELLERTM 36XW-CTD; EC accuracy of ≤ ±2.5%; T with accuracy of ≤ 0.1°C for the pressure head). To quantify low discharge (Q) with high resolution, a tipping bucket rain gauge was installed under the outlet of the weir and used additional to hand measurements to correlate to the Q rate. The total water volume during each hydrological event of interest was summed up (called "Q total volume") and, in addition, the event volume was calculated, which corresponds to the total volume minus the base flow (called "Q event volume"). A smaller chimney nearby with an overburden of 13 m at its narrow top, and a significantly lower Q, was also equipped with a plastic sheet, to collect the drip water and measure Q with another tipping bucket rain gauge. Air temperature in the cave was measured at the weir with one Niphargus logger (resolution ±0.01°C, Burlet et al. 2015).

2.2.3 | Geophysical Measurements

ERT monitor differences in water saturation in the subsoil during the snowmelt period of 3 weeks, with an interval of 7 h,

resulted in 71 time lapses. The electrical conductivity (σ) of the subsurface is controlled by three conduction mechanisms (e.g., Niggli 1948): Matrix conduction is negligible in media without electrical conductors (i.e., metals) and is not considered in this study. Electrolytic conduction (σf) refers to the migration of electrical charge through the water present in the pores and fissures (i.e., the ions dissolved in the electrolyte filling the pore space) and depends on the porosity, water saturation and concentration as well as charge and mobility of the ions. Surface conductivity (σs) refers to the accumulation and polarisation along the electrical double layer formed at the grain-liquid interface and depends on surface area and surface charge of the grains. Electrical conductivity is the inverse of the electrical resistivity ($\rho = 1/\sigma$), which is used in this study. In the case of karstic environments, typical geological materials of the host rocks (e.g., limestones and dolomits) are associated with a wide range of electrical resistivity values ($0.05 < \rho < 10\,000\,\text{k}\Omega\text{m}$, e.g., Reynold 1997), strongly influenced by water saturation.

Galvanised steel screws (6 cm long, for 6 mm holes) act as electrodes and are used to attach the cable to the cave walls or ceiling (Figure 2f). The coordinates of the 96 electrodes were recorded using a DistoX (Heeb 2014). For the collection of the ERT measurements, we used a Lippmann 4-point light instrument, performing measurements in a dipole–dipole configuration with 2025 quadrupoles. For the forward modelling of the data, we used CRTomo (Kemna 2000). This is an iterative smoothness-constraint inversion algorithm and is controlled by specifying a confidence level given by the data error. In CRTomo, the inversion stops when the modelled resistances are equal to the measured resistances weighted by the associated error parameter, that is, when the error-weighted RMS (root-mean-square error) is equal to one. CRTomo uses a linear relationship between the measured values (R) and their errors (s_R):

$$s_R = \text{a} + \text{bR}$$

where a is the absolute error (in Ω), relevant for low resistance values and b is a relative error (in percent), important for higher resistance values (LaBrecque et al. 1996). As reciprocal readings were not feasible due to limited time during the monitoring, outliers were identified by means of the analysis of histograms (e.g., Flores Orozco et al. 2018), which represent the distribution of the recorded data. The examination of the histograms of all 71 measurements (t1–t71) has revealed a common threshold value of 250 Ω for the maximum accepted resistances, with all readings exceeding this considered as outliers. To make all measurements comparable, the quadrupoles present in all 71 measurements were extracted, resulting in a total of 451 quadrupoles. The best results after inversion (resulting in an RMS equal to 1) for all profiles were achieved defining a relative error of 40% and an absolute error of 2 Ω. In this study we blank out model parameters in the imaging results with a cumulative sensitivity that is 2 orders of magnitude smaller than the largest cumulative sensitivities (e.g., Weigand et al. 2017; Flores Orozco et al. 2013).

As ERT measurements are highly dependent on T (e.g., Hermans et al. 2014; Caterina et al. 2017; Fäth and Kneisel 2024), all measurements were corrected to a common T of 10°C, using the measured T at a soil depth of 3 cm: $\rho_t = \rho \cdot (1 + \alpha \cdot (T - 10))$, where ρ_t corresponds to the resistivity at 10°C and α was chosen as 0.025 according to Ward (1990). As the data are T corrected and a change in the properties of the subsoil (i.e., porosity, properties of grains, ...) within a few weeks can be neglected, we interpret any changes in the imaging results to be attributed to the degree of water saturation.

ERT imaging results in 2D images of the subsurface resistivity between the cave and the surface. We divided these images into three zones (Figure 2). The soil zone is approximately 2–3 m deep and includes the soil layer and the uppermost part of the more weathered and fractured zone (epikarst). The cave zone corresponds to the fractured zone near the ceiling of the cave in the upper vadose zone. The bedrock zone is defined as the region in between, which belongs to the upper vadose zone and consists of the porous bedrock and conduits (dual flow system).

3 | Results

3.1 | Data Overview

The measurements between February to mid-August 2024 were carried out in a relatively mild winter, with high winter T in February (at Hochschwab avarage T was 4°C higher than the annual average between 1991 and 2020) and a significant T drop in mid-April (Figure 1). During the snowmelt monitoring, snow together with three effective rain events (at the rain gauge) could be observed (Figure 3). In spring and early summer, there were an exceptionally high number of P events, resulting in a rainy June. In July and August, longer dry periods alternated with heavy P, accompanied by exceptionally high T, leading to the warmest August in measurement history in the lowlands and in the mountains of Austria (Geosphere Austria 2024) with an average T of 12°C at the cave.

In February and March, soil T (20 cm) was around 0°C and increased at the beginning of April. VWC sensors at different locations and depths show the same trend, but different amplitudes (content variations due to soil properties) and response times to events. At each location, the response to the event is delayed with increasing depth. VWC is given and discussed for location 2 at 5 cm depth as an example, VWC varies between 0.28 and 0.55 m^3/m^3 representing dry and wet conditions, respectively.

In the cave, T below freezing were observed and resulted in a freezing of the weir causing a gap in the time series of Q and EC at the beginning of March (Figure 3). At the weir, minimal Q of 0.3 mL/s was observed during winter and after long dry periods. The snowmelt infiltration started at the beginning of March, whereby snowmelt infiltration resulted in lower Q (up to 40 mL/s and a mean discharge of 5 mL/s during the snowmelt monitoring) compared to heavy rain events with a maximum of 1440 mL/s at the weir. Between April and August, the mean Q is 10 mL/s and 10 rain events resulted in Q above 100 mL/s. During the entire investigation period (February to August), 515 m^3 of water was fed into the karst system via the discharge station in the cave, of which only 47 m^3 could be attributed to daily fluctuations in snowmelt. Snowmelt thus accounts for about 10% of the discharge at the measuring weir during this investigation period from February to August.

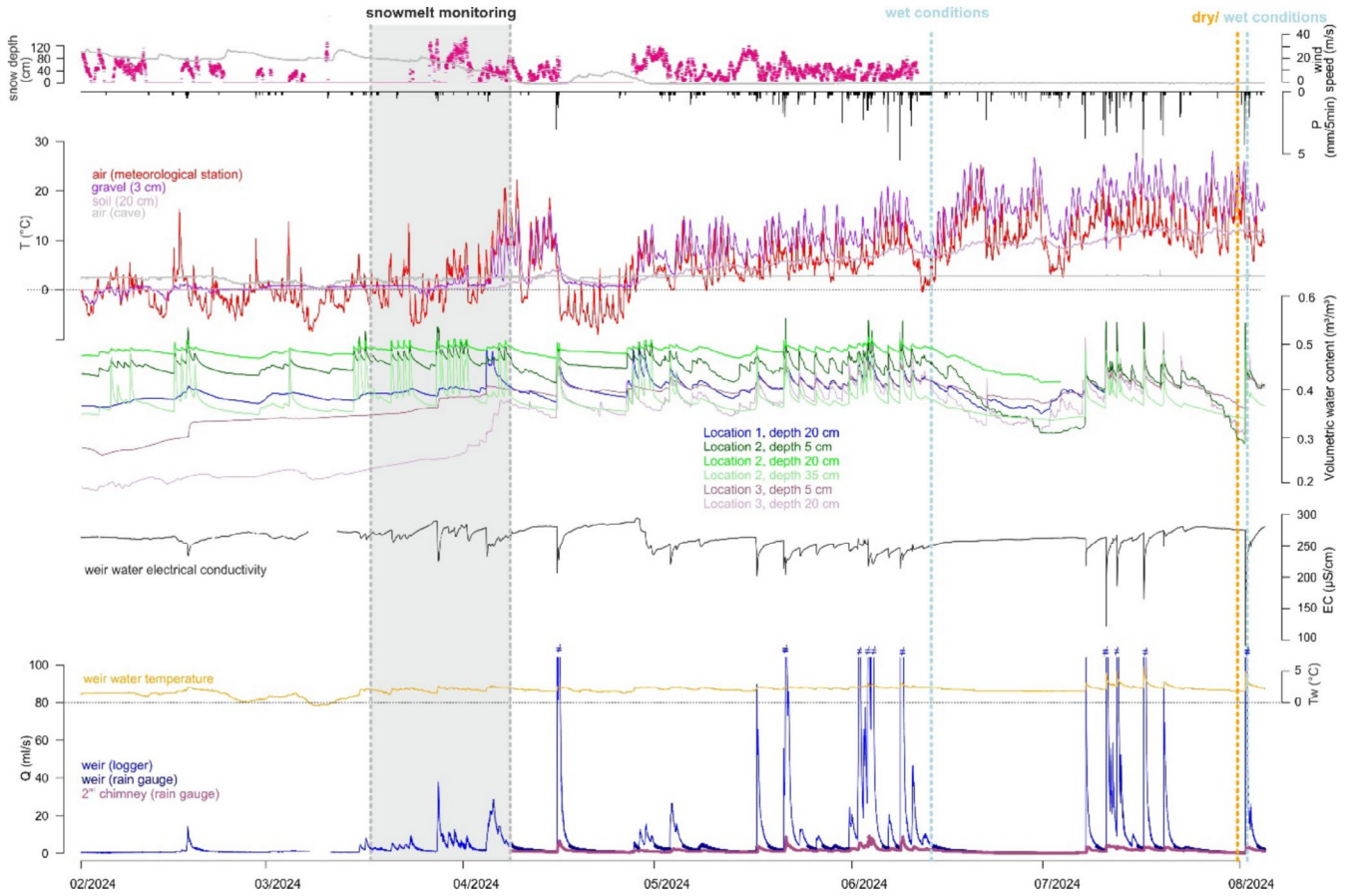

FIGURE 3 | Time series for precipitation (black), temperature (air at the meteorological station at the cave, gravel at 3 cm depth, soil at 20 cm depth, and air in the cave close to the weir), volumetric water content, discharge (Q, the top of the peaks above 100 mL/s were cut off and marked with ≠), water electrical conductivity (EC) and temperature of the water at the weir (T_w); and discharge at the second chimney. Snow depth is monitored at the Sonnschienalm station and wind speed at Hochschwab/Eismauer station. The period of ERT snowmelt monitoring is shown in grey. The blue and orange dotted lines indicate the time of ERT measurements during the summer monitoring.

Less water was collected in the second chimney and the average Q was 1.3 mL/s (0.06–9 mL/s) but the trend is similar to the measurements at the main chimney. EC fluctuations, with a mean of 262 µS/cm during snow melt and rain phases, suggest that freshly infiltrated water also arrived and not only stored water from previous events. The mean water temperature was 2°C and increased significantly with heavy rain events to a maximum of 5.8°C.

3.2 | Snowmelt Monitoring (March/April 2024)

Continuous monitoring of snowmelt was conducted during the longest snowmelt period at the cave in 2024, which lasted about 3 weeks (Figure 4). The snow depth at the Sonnschienalm (weather station at 1524 m) showed a continuous snow cover (Figure 3). However, it is assumed that the amount of fresh snow in the catchment area is less than 50% of the fresh snow at the Sonnschienalm station due to the high wind drift potential in the catchment area (Figure 3, wind speed at Hochschwab/Eismauer). Regular visits to the case study area during the monitoring period (Figure 5, grey arrows) showed partial snow cover of the study area (similar to Figure 5a) with similar patterns to those observed at the weather station on the Sonnschienalm. At the beginning of the monitoring (March 17), the snow depth was on average 5–10 cm (field observation), while at the Sonnschienalm station it was 80 cm. This decreased continuously until March 23, followed by fresh snow resulting in a higher snow depth (10 cm) on March 27. The snow depth continuously decreased until April 8 and there was still snow in some dolines during the last fieldwork (April 8). A rough estimation of the total snow depth (beginning of monitoring plus 50% of fresh snow amount at Sonnschienalm station) of 20 cm, a catchment size of 60 m^2 and a density of 350–400 kg/m^3 for wind packed snow (Paterson 1994) results in a total snow water equivalent (SWE) of 4.2–4.8 m^3 during the snowmelt monitoring period.

Table 1 shows the total discharge volume of each event at the weir, the event volume (total discharge minus baseflow) and, to distinguish between snowmelt and P, the estimate of the P contribution during snowmelt (P fraction of Q). The water volume of P was calculated based on the size of the catchment (60 m^2 according to Zemann 2024), and the remaining event water is assigned to snowmelt. Daily air temperature cycles correspond to the daily variation of discharge with short time lags of the peaks. Event 7 (Figure 4) is such a snowmelt event as no precipitation occurred. For snowmelt, the typical Q event volume varies between 38 and 430 L, while mixed events (snowmelt and precipitation) fluctuate more. The sum of the

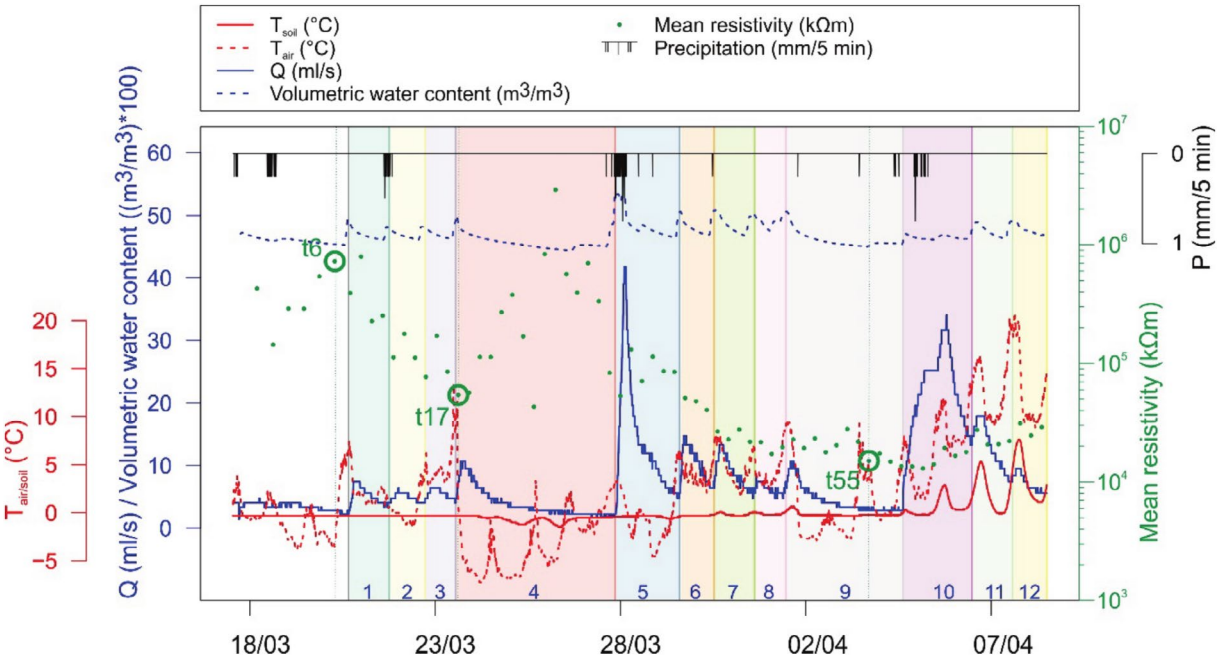

FIGURE 4 | Discharge measurement (blue line) at the weir of the main chimney, volumetric water content (blue dashed line) at location 2 in 5 cm depth, air temperature (red dashed line) and soil temperature (20 cm depth, red line), mean resistivity (each ERT measurement takes 3 h, green dots) and precipitation (black bars). In total, 12 discharge events are differentiated (background colours and blue numbers) and the ERT images given in Figure 6 (t6, t17 and t55) are marked (green circles).

snowmelt event volume during the entire snowmelt monitoring was 5.4 m^3, which is slightly higher than the assumed SWE of 4.2–4.8 m^3 based on meteorological assumptions. With the increase of air T, P also occurred next to the snowmelt, leading to significant increases in discharge at event 5 (March 28) and 10 (April 5). Due to the wind (up to 40 m/s) during events 5 and 10, P measurements may be incorrect here, and a clear distinction between P and snowmelt is uncertain. In event 5 (Figure 4), 13 mm of P contributes to 43% of Q volume, whereas for event 10, 4 mm of P results only in 8% of the total Q volume. P cannot be clearly categorised for the first two events, as P occurred just before the second event (Figure 4), but its hydrological response at the weir (Q, EC, and water T) matches the response during snowmelt. A typical response to snowmelt at the weir results in discharge fluctuations between 2 and 15 mL/s, a slight decrease in EC, and an increase in water T (Table 1 and Figure A2). The VWC usually starts to increase 2 to 4 h before the observed increase in discharge at the weir, except for events influenced by P.

The ERT monitoring (Figure 5) generally shows good agreement with the hydrological measurements. Under dry conditions (e.g., March 20 or 26) there is a clear maximum in resistivity, while resistivity decreases as conditions become wetter. The ERT snowmelt monitoring shows a continuous saturation in the studied area over the entire period, especially in the bedrock zone (Figure 5). Snowmelt water infiltration due to diurnal T cycles can be observed in the resistivity and also in the Q and VWC (Figure 4). At the beginning of the ERT monitoring, no new snowmelt water infiltrated due to a cold front, which led to a short-term increase in resistivity (t6). After t6, temperature increased and led to snowmelt until t17 (March 23). The next recharge event was snowmelt in combination with rain on March 28, resulting in an increasing water saturation of all zones with daily snowmelt events until April 2. With the rising T on the following day (t55), water infiltration could be observed again and led according to the ERT to a similar saturation of the bedrock zone as on April 2, and the maximum saturation of the bedrock zone without the influence of rain was reached (Figure 5, t55). A further increase in saturation of the bedrock zone is associated with rain in addition to the snowmelt, resulting in a minimum resistivity on April 5 corresponding to the maximum water saturation in all zones (Figure 5). The extreme increase in Q is due to P, and faster snowmelt caused by higher T (Figure 4). The comparison between the total P and the total Q at the measuring weir shows that this P event (10) only accounts for 8% of the Q. The higher saturation in the bedrock and in the epikarst before event 10, and the continuous increase in resistivity during the event, especially in the bedrock zone, can explain that a large fraction of the discharge comes from the stored water. The maximum saturation in the bedrock zone lasts for 42 h.

The cave zone shows low fluctuations in the mean resistivity from March 28 (Figure 5). This suggests that the cave zone has reached its maximum possible saturation during the observation period. Here the cave zone is continuously recharged with water from the bedrock zone. The mean resistivity of the soil zone generally shows a faster response to events and only short-term trends towards higher saturation (e.g., between March 29 and April 1). The abrupt rise in the mean resistivity on April 7 (Figure 5, t64 to t65, red arrow) marks the end of snowmelt along the ERT profile, while VWC and Q show that there are still some areas where snowmelt is occurring. As T rises, the soil zone, as well as the bedrock zone, but not yet the cave zone, begins to dry out.

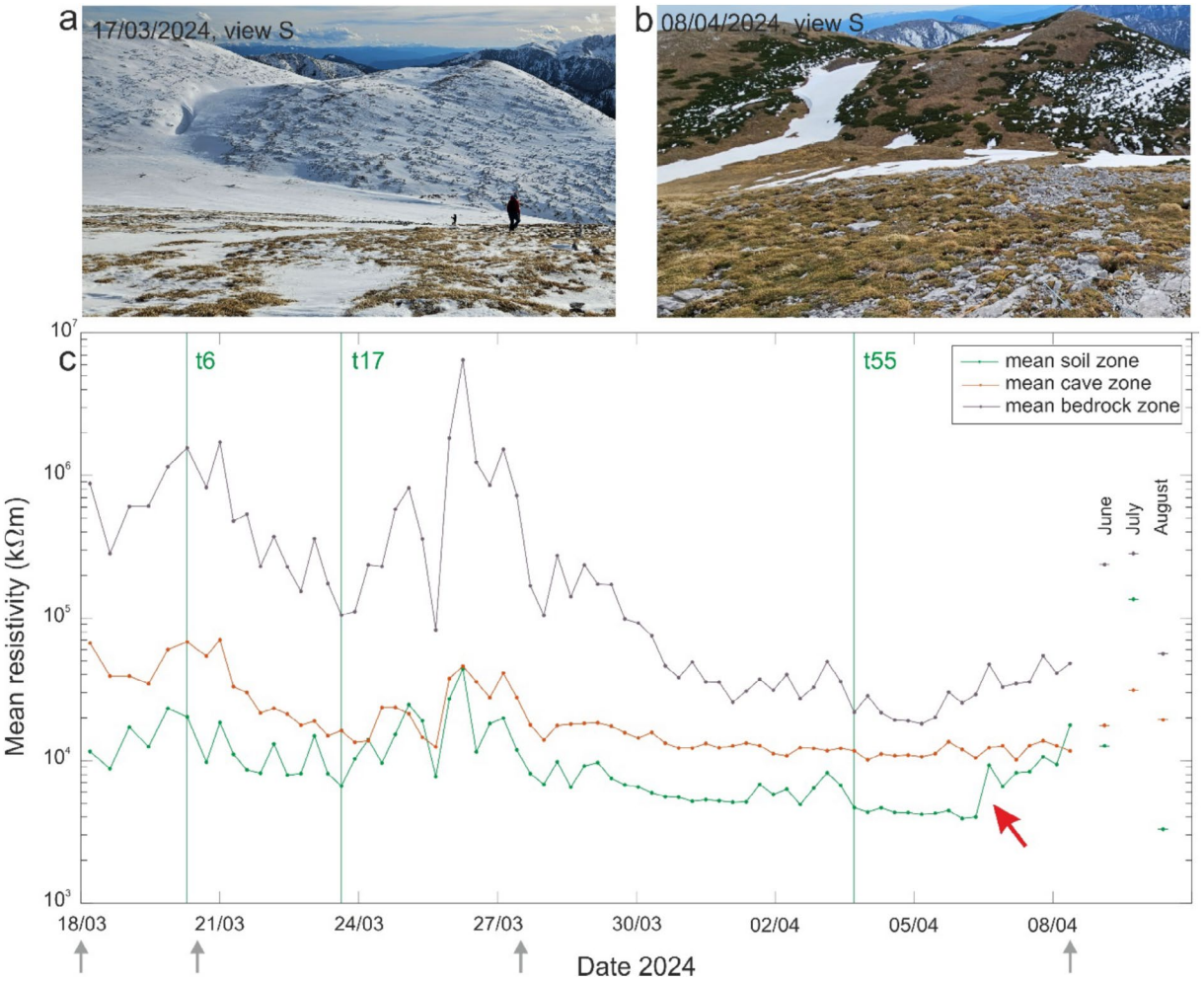

FIGURE 5 | Surface conditions at the beginning (a) and end (b) of the snowmelt monitoring period are shown in the two photos. Trend of mean resistivity in the three zones during snowmelt as well as for the three summer events (c). The red arrow indicates the time when the snowmelt stops at the ERT profile. Green lines give the dates of the three shown resistivity images and grey arrows mark the times, where snow cover depth was checked in the field. The cave entrance is at the position of the lower person in Figure 5a, a detailed overview of the sensor position is given in Figure S1.

3.3 | Summer Dry/Wet Conditions

In summer, two P events with varying intensities and a dry period were investigated in detail (Table 2). The P events were distinguished by their distinct characteristics. The first one (on June 13) marked the end of a 14-day period of rain; the second was a heavy summer thunderstorm. The wet events show increased VWC values of 0.43 and 0.45 m^3/m^3, which are above the mean (0.43 m^3/m^3) and close to the upper 10th percentile (0.47 m^3/m^3). In total, 10 and 2 days before the event in June, 162 mm and 18 mm of P (characterised by heavy and light rain over several hours) were observed (Table 2). During the ERT measurement (in June), light rain continued, but VWC and Q had already begun to decline from their peak levels (Figure 3). The EC of the water at the weir was increasing, indicating that no fresh rainwater was infiltrating (Figure 3). From the comparison with the snowmelt monitoring (Figure 5) it can be concluded that the soil zone and the cave zone were slightly, and the bedrock zone clearly less saturated than the maximum saturation reached during the snowmelt period.

On August 2, the second wet monitoring was carried out at the cave during a heavy rainfall event with a total P of 26 mm/d (the Sonschienalm meteorological station showed $P\,sum > 60$ mm/d). There was no effective P (> 2 mm) for 10 days prior to this event. Discharge responded very quickly (< 30 min) to the P, up to a maximum of 1.1 L/s, and the lowest EC (91 µS/cm) of the weir water, illustrating the fast flow component in the karst. ERT monitoring was conducted before the event (July 31) and within the falling peak of the Q (35 mL/s). The VWC was 0.43 m^3/m^3 on average during the ERT monitoring (Table 2). In contrast to the June event, the soil zone showed a higher level of saturation, while the cave and bedrock zones did not reach the same level of saturation as during the snowmelt period.

Dry monitoring was carried out on July 31 with no effective rain falling for 7 days. The dry conditions are also indicated by the low Q (0.3 mL/s) and VWC of 0.31 m^3/m^3, which is below the lower 10th percentile (0.36 m^3/m^3) of the measured values in the time series. Also, the ERT monitoring shows low saturation in all three zones.

TABLE 1 | Hydrological snowmelt monitoring event classification.

Event	pET (mm)	P sum (mm)	Q total volume (L)	Q event volume (L)	P_fraction of Q (–)[a]	Snowmelt event volume (L)	EC mean change (µS/cm)	Tw mean change (°C)	Q beginn (mL/s)	EC beginn (µS/cm)	Tw beginn (°C)	VWC (m^3/m^3)
1	1.0	3.5	489	275	0.76	65	−12	0.55	2	275	1.50	0.47
2	0.5	0.5	408	126	0.24	96	−2	0.12	3	267	2.00	0.47
3	0.5	0.0	395	107	—	107	−3	0.11	4	268	2.10	0.47
4	0.8	0.0	1431	287	—	287	12	−0.29	4	266	2.20	0.46
5[b]	0.9	12.8	2059	1789	0.43	1024[b]	−23	0.77	2	289	1.50	0.49
6	0.6	0.0	813	430	—	430	−7	0.18	5	280	2.10	0.48
7	1.0	0.3	832	309	0.05	294	−3	0.03	6	276	2.20	0.49
8	0.9	0.0	458	112	—	112	0	0.03	5	281	2.10	0.49
9	1.8	1.3	1199	182	0.41	107	−11	0.02	5	284	2.00	0.46
10[b]	2.1	4.3	3448	3000	0.08	2745[b]	−26	0.61	3	278	1.90	0.46
11	1.8	0.0	1213	132	—	132	−1	−0.06	13	263	2.50	0.48
12	2.0	0.0	566	38	—	38	0	−0.06	7	265	2.40	0.48

Abbreviations: EC = water electrical conductivity; Tw = water temperature; *P* = precipitation (P effective > 2 mm); pET= potential evapotranspiration; Q = discharge, Q event volume = Q total volume – Q baseflow; VWC = mean volumetric water content at L2 in 5cm.

[a]Catchment size of 60 m^2 is used (Zemann 2024).

[b]Measurement errors in precipitation are possible due to high wind speeds and results are not reliable.

TABLE 2 | Overview of the summer monitoring conditions at the weir in terms of discharge (Q), water electrical conductivity (EC), water temperature (T_w), volumetric water content (VWC), precipitation sum of different days prior to the event (P sum), and mean electrical resistivity of each zone.

Event type	Wet	Dry	Wet
Measurement date	13/06/2024	31/07/2024	02/08/2024
Q (mL/s)	6.4	1.04	30.4
Q total volume during ERT measurement (L)	71	11	337
Q total volume of 24 h until end of ERT measurement (L)	692	90	6775
EC (μS/cm)	252	276	237
Tw (°C)	2.4	1.9	3.4
VWC at L2_5cm (m^3/m^3)	0.45	0.31	0.43
P sum 10 days (mm)	162	14	29.25
P sum 5 days (mm)	87.5	1	27.25
P sum 2 days (mm)	17.5	0	26.25
P sum measurement (mm)	1.5	0	0
Mean resistivity soil zone (kΩm)	13	135	3.3
Mean resistivity cave zone (kΩm)	18	31	19
Mean resistivity bedrock zone (kΩm)	251	267	56

Note: Q, EC, T_w, VWC, P sum measurement is given as mean of ERT measurement period (3 h).

3.4 | Comparison of Water Infiltration Processes

Figure 6 shows spatial saturation variations with the ERT images for three snowmelt and three summer events. For both, we show one image under dry and two under wet conditions. An animation of all ERT snowmelt monitoring images is given in the Supporting Information: S2. Figure 6 reveals the following three units: (i) low resistivity values ($\rho < 1$ kΩm) mainly corresponding to the soil at the surface; (ii) intermediate to high resistivity values ($1 < \rho < 30$ kΩm) show fractured zones below the surface as well as at the cave walls and ceiling; (iii) high resistivity values ($\rho > 30$ kΩm) correspond to the mainly compact rock body, where small changes in resistivity can be attributed to differences in the sensitivity of the individual measurements. Dry conditions for both monitorings are given in Figure 6a,d. In both measurements, the bedrock zone shows high resistivity values (> 100 kΩm). While the bedrock is dry over a large area in winter (Figure 6a), it still has some moisture in summer, especially at the border to the cave zone (Figure 6d), as indicated by lower resistivity values. This suggests that water from previous rainfall (heavy rain events in June) is slowly draining towards the cave zone. In the soil zone, the imaging result for July (Figure 6d) shows the higher resistivity values, caused by the drying out of the soil due to high T, resulting in transpiration and evaporation. The large differences in the soil zone are related to in homogeneities in the soil and epikarst.

We compare a resistivity image after the first prolonged period of snowmelt (Figure 6b) and after a longer period of rain (Figure 6e). For both events, the monitoring of the mean discharge and the discharge volumes within the last 24 h were in the same range. Both images show low resistivities (< 1 kΩm) in the soil as well as in most areas of the cave zone. However, the soil zone shows a higher saturation (i.e., lower resistivity values) in the summer image (Figure 6e) than in the snowmelt image (Figure 6b). The bedrock zone shows a fairly high resistivity in both images, suggesting that no deep saturation has occurred yet.

Figure 6c,f compare the latest snowmelt image, without the influence of rain events and a summer image measured immediately after a heavy thunderstorm. A clear difference can be seen in the bedrock zone. After 2 weeks of snowmelt, the bedrock zone reached a much higher degree of saturation than after a single heavy rain event (Figure 6f) as well as a long period of rain (Figure 6e). Q, on the other hand, is higher during summer events than during snowmelt events (Figure 6, Q values).

4 | Discussion

4.1 | Methodical Limitations

In this study, various methods were used at different scales to better understand the process of water infiltration, especially during snowmelt. However, each method has its own limitations. Frost and high T in summer must be taken into consideration as a further source of error for the following reasons: Sensors in the weir, rain gauges and VWC sensors will not give meaningful results if the ground or water is frozen. The ERT measurements are corrected by the T value of the soil at a depth of 3 cm, but the T differences along the profile are unknown and therefore cannot be considered for the T correction. The conductivity of the subsoil is influenced by the EC of the water, with the EC of infiltrating rainwater expected to increase slowly as it infiltrates the epikarst. While several studies assumed constant pore-water conductivity (e.g., Beff et al. 2013; Garré et al. 2011; Michot et al. 2003) others showed an uncertainty in the calculation of moisture content variations with ERT data (Uhlemann et al. 2016; Watlet et al. 2018) and justified this by the increase in the EC of the water. In this study, the magnitudes in water saturation are several orders of magnitude larger than the variations in EC of the cave drip water (mean 262 μS/cm) and P (20 μS/cm during the rain event), allowing us to neglect the influence of EC variations.

The estimated water recharge at the weir from snowmelt during the observation period was about 5.4 m^3, as derived from the runoff records. However, this estimate may be slightly overestimated due to two P events. Although attempts were made to separate the contributions of P and snowmelt based on

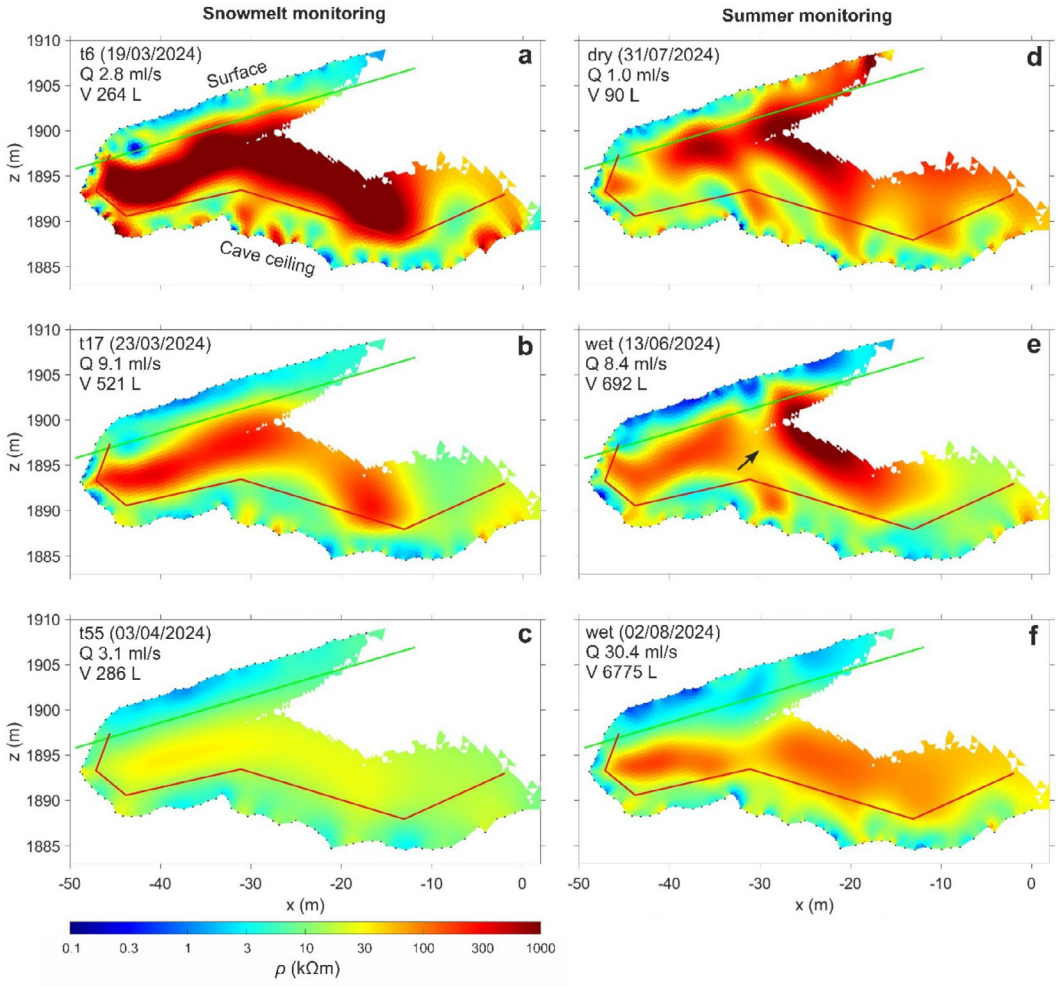

FIGURE 6 | Selected resistivity images during the snowmelt monitoring (a–c) and the summer monitoring (d–f). The green line indicates the contact of the soil and the bedrock zone and red lines show the contact between the bedrock and the cave zone. Discharge (Q) is given as mean during the ERT measurement (3 h) and total discharge volumes (V) of the last 24 h. The black arrow in (e) indicates the position of a fractured zone.

meteorological data over the catchment area, strong winds may have affected the accuracy of the rain gauge's precipitation measurements. Taking this potential error into account, the actual recharge from snowmelt is likely to be in the range of 4.2–4.8 m^3, which is in good agreement with SWE estimates derived from meteorological data.

4.2 | Recharge Processes in the Upper Vadose Zone

According to Klimchouk (2004), a mature epikarst (covered by soil), such as that found at our study site, has high porosity, permeability and storage capacity. At the cave the thickness of the soil varies between 10 and 40 cm (Exel 2014) and contributes as an important function to water storage. Figure 6 shows that both the soil and epikarst become saturated up to 3 m deep over the seasons, which indicates a well-developed epikarst. As previous studies have shown, the relationship between the epikarst and the soil as well as the development of the epikarst is crucial for water storage. Meeks and Hunkeler (2015) suggested that water storage due to soil moisture is more likely to occur in the soil than in the epikarst. Eeckman et al. (2024) showed in winter a decreasing surface water content in the soil and only a minor influence of the melt flux at a depth of 30 cm, but a rapid stream discharge response to snowmelt. In contrast, the soil layer reacts quickly to summer precipitation.

Our study has observed seasonal and spatial variations in water saturation and recharge to the weir. Although the discharge measurements at the cave weir enabled us to quantify the amount of water passing the weir, this amount alone is not a reliable indicator of water saturation variations in the upper vadose zone. The variations in the resistivity, as shown in the 2D ERT images of the soil and upper vadose zone, enabled us to jointly interpret different water recharge events with regard to water saturation in different zones (soil, cave, and bedrock). For example, the ERT data in Figure 6b,e, were observed at similar discharge volumes. However, the ERT image of Figure 6b (snowmelt) indicates more uniform and deeper water saturation during snowmelt, whereas Figure 6e shows a higher saturation in the soil and in preferential flow paths after rain. This illustrates how inflow dynamics influence the volume of stored water. Accordingly, the event with the highest discharge volume (6775 L during a rainfall event) resulted in an increase in water saturation of the soil and epikarst. Thus, P led to a rapid throughflow, with a high volume at the weir.

The rapid infiltration processes can be observed over the course of the seasons at the weir due to the well-developed karst features, which are facilitated by the high porosity and permeability of the system (Figure 3). Q from both hydrological stations is adequately characterised by a dual, karst-typical discharge regime. The observed Q remains at a low but constant level during prolonged dry periods, indicating a storage component. The rapid response to precipitation shows the presence of a rapid discharge component. The connected channels in the vadose zone have a relatively short residence time, while the filtering effect is rather low, making the catchments highly vulnerable to pollutants (e.g., Dvory et al. 2018; Hartmann et al. 2021).

In contrast to the rapid infiltration, 15 days of snowmelt resulted in lower discharge rates than rain (e.g., 286 L/24 h, Figure 6c), but the highest homogeneous saturation of the bedrock zone, with resistivities down to 10 kΩm. This is one order of magnitude lower than after rainfall (100 kΩm in the bedrock, Figure 6e) and suggests that continuous, low snowmelt promotes the gradual and widespread infiltration of water into the subsurface. Here, the diffuse recharge of snowmelt enables a deep saturation of the pores and small fissures in the bedrock as long as the system continues to be enriched with water.

The following observations allow the snowmelt dynamic in the different zones to be interpreted: After the start of the snowmelt, the resistivity in the cave zone reaches a minimum value due to continuous recharge from the zones above, and remains until the end of the snowmelt monitoring. We interpret this as the maximum saturation of the cave zone. Wet summer conditions also show lower resistivities in the cave zone, that is, more humid conditions, but do not reach the same minimum value as after the snowmelt. The cave zone includes frost-weathered fissures (Gelifracts) and fractures at the cave ceiling and always has a lower resistivity, like the epikarst. Gelifracts and the occurrence of cryogenic cave carbonates indicate a freezing of the whole cave during Pleistocene cold periods (Plan et al. 2019), and even today frost can be observed from the entrance beyond the two chimneys during cold winter periods. It is supported by the low T in the cave air and the strong wind in the cave in winter (field observation), which also led to the temporary freezing of the measuring weir (e.g., Figure 2 gap in the data) and to frost weathering of the fractured zone. Such frost weathering processes are commonly observed in fractured karst zones (e.g., Deprez et al. 2020; Sass 2004). However, inhomogeneities caused by tectonic structures, for example, fault zones, are likely in the host rock. The fault zones can be a reason for the spatial differences in the ERT image (black arrow in Figure 6e bedrock zone).

At the end of the ERT snowmelt monitoring, the bedrock zone dries out again as the water percolates downwards. The longest water saturation during snowmelt takes place in the highly fissured cave zone (area characterised by tectonics and frost weathering). While soils and epikarst show the highest variability in the ERT images between dry and wet summer conditions (Figure 6, right column), consistent with Watlet et al. (2018), the highest variability of resistivity (and thus saturation) during snowmelt is seen in deeper regions (Figure 5, bedrock zone), where it varies by about two orders of magnitude.

5 | Summary and Conclusions

This study shows that the duration and rate of water infiltration are of crucial importance for water saturation in the upper vadose zone of an Alpine karst. During the three-week snowmelt observation period, meteorological assumptions were used to determine a SWE at the karst catchment, which was found to be between 4.2 and 4.8 m^3. This is slightly below the estimated total snowmelt volume of 5.4 m^3 at the cave drip water. Only after 15 days of slow and continuous saturation by snowmelt (and few P events during this period) with a mean discharge of 5 mL/s in the cave is a deep saturation in the solid rock (bedrock zone) observed with ERT measurements. This could not be achieved either after a long period of rain (10 m^3 for a 60 m^2 catchment in 10 days) or through summer thunderstorms (1.5 m^3 in 3 h). On the other hand, summer P infiltration results in a high *Q* value of up to 1440 mL/s at the weir, showing rapid and quick water flow to the weir. However, ERT data did not suggest that the bedrock zone was deeply saturated. The increase in discharge volume at the weir due to precipitation infiltration is also confirmed by the decrease in water electrical conductivity and the increase in water temperature. This study suggests that snowmelt, with its slow infiltration, is important for the slow formation of groundwater with a natural purification of the water. Due to the expected shortening of the snowmelt period as a result of climate change, the slow groundwater recharge is at risk. The time lag during snowmelt events between T rise, increasing soil moisture, and the arrival of drip water in the cave illustrates the complexity of the flow paths and the temporal sequence of water movement within the vadose zone. The various sensors enabled us to record specific hydrological processes: soil moisture sensors indicated fluctuations in soil water saturation, while geophysical monitoring revealed saturation changes and water storage patterns with a coarser resolution over a larger spatial scale down to the rock level. Considering the inflow into the entire karst system and the cave drip water as natural lysimeters, most of the recharge occurs via fast flow paths, especially in summer. This is indicated by high volumes measured at the weir. The total snowmelt contribution within the studied time period (February to August) was only about 10%. Only the combination of meteorological, hydrological, and geophysical (ERT inversion images) data allowed these observations.

Acknowledgments

The authors thank the support of the Austrian Science Fund (FWF): P36065-N. E.K. thanks the support of the Hochschuljubiläumsfonds: H-912466/2022. B.F. thanks the support of the Hochschuljubiläumsfonds: H-876947/2022. The team would like to thank Dieter Sulzbacher and Thomas Exel for the installation of the measuring weir and meteorological station at the cave. Johannes Rabl and Paul Zemann are thanked for pre-investigations. Michael Nagl, Lina Rummler, Richard Michtner, and Helene Bauer are thanked for the support in the field. For scientific discussions, thanks to Pauline Oberender. We would like to thank MA31 Wiener Wasser and GeoSphere Austria for the provision of data. We thank the referees for their comments to improve the manuscript. N/A

Data Availability Statement

The data that support the findings of this study are openly available in NHMW Data Repository at https://datarepository.nhm-wien.ac.at/.

Meteorological data has to be requested by MA 31 Wiener Wasser and GeoSphere Austria.

References

Arbel, Y., N. Greenbaum, J. Lange, and M. Inbar. 2010. "Infiltration Processes and Flow Rates in Developed Karst Vadose Zone Using Tracers in Cave Drips." *Earth Surface Processes and Landforms* 35, no. 14: 1682–1693. https://doi.org/10.1002/esp.2010.

Bauer, H., T. C. Schröckenfuchs, and K. Decker. 2016. "Hydrogeological Properties of Fault Zones in a Karstified Carbonate Aquifer (Northern Calcareous Alps, Austria)." *Hydrogeology Journal* 24, no. 5: 1147–1170. https://doi.org/10.1007/s10040-016-1388-9.

Beff, L., T. Günther, B. Vandoorne, V. Couvreur, and M. Javaux. 2013. "Three-Dimensional Monitoring of Soil Water Content in a Maize Field Using Electrical Resistivity Tomography." *Hydrology and Earth System Sciences* 17: 595–609. https://doi.org/10.5194/hess-17-595-2013.

Berthelin, R., T. Olarinoye, M. Rinderer, et al. 2023. "Estimating Karst Groundwater Recharge From Soil Moisture Observations-a New Method Tested at the Swabian Alb, Southwest Germany." *Hydrology and Earth System Sciences* 27, no. 2: 385–400. https://doi.org/10.5194/hess-27-385-2023.

Binley, A., S. S. Hubbard, J. A. Huisman, et al. 2015. "The Emergence of Hydrogeophysics for Improved Understanding of Subsurface Processes Over Multiple Scales." *Water Resources Research* 51, no. 6: 3837–3866. https://doi.org/10.1002/2015WR017016.

Brussolo, E., E. Palazzi, J. von Hardenberg, et al. 2022. "Aquifer Recharge in the Piedmont Alpine Zone: Historical Trends and Future Scenarios." *Hydrology and Earth System Sciences* 26, no. 2: 407–427. https://doi.org/10.5194/hess-26-407-2022.

Bryda, G., D. van Husen, O. Kreuss, et al. 2013. "Erläuterungen zu Blatt 101 Eisenerz." Geologische Bundesanstalt, A-1030 Wien, Neulinggasse 3.

Burlet, C., Y. Vanbrabant, K. Piessens, K. Welkenhuysen, and S. Verheyden. 2015. "Niphargus: A Silicon Band-Gap Sensor Temperature Logger for High-Precision Environmental Monitoring." *Computers and Geosciences* 74: 50–59. https://doi.org/10.1016/j.cageo.2014.10.009.

Carriere, S., K. Chalikakis, C. Danquigny, R. Clement, and C. Emblanch. 2015. "Feasibility and Limits of Electrical Resistivity Tomography to Monitor Water Infiltration Through Karst Medium During a Rainy Event." *Environmental Earth Sciences* 1, no. 1: 45–55. https://doi.org/10.1007/978-3-642-17435-3_6.

Carrière, S. D., and K. Chalikakis. 2022. "Hydrogeophysical Monitoring of Intense Rainfall Infiltration in the Karst Critical Zone: A Unique Electrical Resistivity Tomography Data Set." *Data in Brief* 40: 107762. https://doi.org/10.1016/j.dib.2021.107762.

Caterina, D., A. Flores Orozco, and F. Nguyen. 2017. "Long-Term ERT Monitoring of Biogeochemical Changes of an Aged Hydrocarbon Contamination." *Journal of Contaminant Hydrology* 201: 19–29. https://doi.org/10.1016/j.jconhyd.2017.04.003.

Cochand, M., P. Christe, P. Ornstein, and D. Hunkeler. 2019. "Groundwater Storage in High Alpine Catchments and Its Contribution to Streamflow." *Water Resources Research* 55, no. 4: 2613–2630. https://doi.org/10.1029/2018WR022989.

De Waele, J., and F. Gutiérrez. 2022. *Karst Hydrogeology, Geomorphology and Caves*. John Wiley & Sons Ltd. https://doi.org/10.1002/9781119605379.fmatter.

Deprez, M., T. de Kock, G. De Schutter, and V. Cnudde. 2020. "A Review on Freeze-Thaw Action and Weathering of Rocks." *Earth-Science Reviews* 203: 103143. https://doi.org/10.1016/j.earscirev.2020.103143.

Djukic, I., F. Zehetner, M. Tatzber, and M. H. Gerzabek. 2010. "Soil Organic-Matter Stocks and Characteristics Along an Alpine Elevation Gradient." *Journal of Plant Nutrition and Soil Science* 173: 30–38. https://doi.org/10.1002/jpln.200900027.

Dvory, N. Z., Y. Livshitz, M. Kuznetsov, et al. 2018. "Caffeine vs. Carbamazepine as Indicators of Wastewater Pollution in a Karst Aquifer." *Hydrology and Earth System Sciences* 22, no. 12: 6371–6381. https://doi.org/10.5194/hess-22-6371-2018.

Eeckman, J., B. de Grenus, F. Miesen, J. Thornton, P. Brunner, and N. Peleg. 2024. "Dynamics of Snow Melt Infiltration Into Mountain Soils: An Instrumental Approach in the Nant Valley, Swiss Alps." August, 1–23.

Einsiedl, F., P. Maloszewski, and W. Stichler. 2009. "Multiple Isotope Approach to the Determination of the Natural Attenuation Potential of a High-Alpine Karst System." *Journal of Hydrology* 365, no. 1–2: 113–121. https://doi.org/10.1016/j.jhydrol.2008.11.042.

Exel, T. 2014. "Abschätzung des Wasserspeichervermögens der Bodenzone und des Epikarsts am Hochschwabplateau (Issue September)."

Exel, T., S. Hermann, F. Ottner, K. Wriessnig, and L. Plan. 2016. "Untersuchungen zum oberflächennahen Wasserspeichervermögen am Hochschwab-Karstplateau." *Die Höhle* 67: 77–87.

Fan, X., N. Goeppert, and N. Goldscheider. 2023. "Quantifying the Historic and Future Response of Karst Spring Discharge to Climate Variability and Change at a Snow-Influenced Temperate Catchment in Central Europe." *Hydrogeology Journal* 31, no. 8: 2213–2229. https://doi.org/10.1007/s10040-023-02703-9.

Fäth, J., and C. Kneisel. 2024. "Combined 2D- and 3D ERT Monitoring as a Geophysical Tool for Investigating Spatial and Temporal Soil Moisture Fluctuations in a Pine-Beech Forest." *Trees, Forests and People* 16: 100555. https://doi.org/10.1016/j.tfp.2024.100555.

Flores Orozco, A., J. Gallistl, M. Bücker, and K. Williams. 2018. "Decay Curve Analysis for Data Error Quantification in Time-Domain Induced Polarization Imaging." *Geophysics* 83: E75–E86. https://doi.org/10.1190/geo2016-0714.1.

Flores Orozco, A., K. H. Williams, and A. Kemna. 2013. "Time-Lapse Spectral Induced Polarization Imaging of Stimulated Uranium Bioremediation." *Near Surface Geophysics* 11: 531–544. https://doi.org/10.3997/1873-0604.2013020.

Ford, D., and P. Williams. 2007. "Karst Hydrogeology and Geomorphology." In *Karst Hydrogeology and Geomorphology*. John Wiley & Sons Inc. https://doi.org/10.1002/9781118684986.

Garré, S., T. Günther, J. Diels, and J. Vanderborght. 2011. "Evaluating Experimental Design of ERT for Soil Moisture Monitoring in Contour Hedgerow Intercropping Systems." *Vadose Zone Journal* 11: 412–424. https://doi.org/10.2136/vzj2011.0186.

Geosphere Austria. 2024. "Monatlicher Klimabericht Österreich 2024." https://www.zamg.ac.at/cms/de/klima/klima-aktuell/klimamonitoring/.

Goldscheider, N., Z. Chen, A. S. Auler, et al. 2020. "Global Distribution of Carbonate Rocks and Karst Water Resources." *Hydrogeology Journal* 28, no. 5: 1661–1677. https://doi.org/10.1007/s10040-020-02139-5.

Hartmann, A., N. Goldscheider, T. Wagener, J. Lange, and M. Weiler. 2014. "Karst Water Resources in a Changing World: Review of Hydrological Modeling Approaches." *Eos, Transactions American Geophysical Union* 69, no. 37: 34. https://doi.org/10.1029/88EO01108.

Hartmann, A., S. Jasechko, T. Gleeson, et al. 2021. "Risk of Groundwater Contamination Widely Underestimated Because of Fast Flow Into Aquifers." *Proceedings of the National Academy of Sciences of the United States of America* 118, no. 20. https://doi.org/10.1073/pnas.2024492118.

Heeb, B. 2014. "The Next Generation of the DistoX Cave Surveying Instrument." *CREG Journal* 88: 5–8.

Hermans, T., F. Nguyen, T. Robert, and A. Revil. 2014. "Geophysical Methods for Monitoring Temperature Changes in Shallow Low

Enthalpy Geothermal Systems." *Energies* 7, no. 8: 5083–5118. https://doi.org/10.3390/en7085083.

Houser, L., T. Bechtel, S. Schaneng, et al. 2016. "Geophysical Mapping of Alpine Karst Groundwater Conduits, Hirschegg, Austria." In *Proceedings of the Geological Society of America*, vol. 48. Geological Society of America. https://doi.org/10.1130/abs/2016AM-284006.

Kaminsky, E., L. Plan, T. Wagner, B. Funk, and P. Oberender. 2021. "Flow Dynamics in a Vadose Shaft – A Case Study From the Hochschwab Karst Massif (Northern Calcareous Alps, Austria)." *International Journal of Speleology* 50, no. 2: 157–172. https://doi.org/10.5038/1827-806X.50.2.2375.

Kemna, A. 2000. "Tomographic Inversion of Complex Resistivity - Theory and Application." Ph.D. thesis. Universität Bonn.

Kemna, A., B. Kulessa, H. Vereecken, and J. Vanderborght. 2002. "Imaging and Characterisation of Subsurface Solute Transport Using Electrical Resistivity Tomography (ERT) and Equivalent Transport Models." *Journal of Hydrology* 267, no. 10: 125–146. https://doi.org/10.1016/S0022-1694(02)00145-2.

Klimchouk, A. 2004. "Towards Defining, Delimiting and Classifying Epikarst: Its Origin, Processes and Variants of Geomorphic Evolution." Speleogenesis and Evolution of Karst Aquifers.

Kuschnig, G. 2001. "Das Karstforschungsprogramm der Wiener Wasserwerke." In *Geologische Bundesanstalt Arbeitstagung 2001*, edited by G. Mandl, 213–219. Geologische Bundesanstalt.

LaBrecque, D., M. Daily, A. Ramirez, and E. Owen. 1996. "The Effects of Noise on Occam's Inversion of Resistivity Tomography Data." *Geophysics* 61: 538–548. https://doi.org/10.1190/1.1443980.

Land Steiermark. 2024. "Klimaatlas Steiermark." https://gis.stmk.gv.at/wgportal/atlasmobile/map/Klimatologie%20-20Meteorologie/Klimaatlas%201970-2000.

Liu, A. W., A. Brancelj, and J. Ellis Burnet. 2016. "Interpretation of Epikarstic Cave Drip Water Recession Curves: A Case Study From Velika Pasica Cave, Central Slovenia." *Hydrological Sciences Journal* 61, no. 15: 2754–2762. https://doi.org/10.1080/02626667.2016.1154150.

Lorenzi, V., C. Sbarbati, F. Banzato, A. Lacchini, and M. Petitta. 2022. "Recharge Assessment of the Gran Sasso Aquifer (Central Italy): Time-Variable Infiltration and Influence of Snow Cover Extension." *Journal of Hydrology: Regional Studies* 41: 101090. https://doi.org/10.1016/j.ejrh.2022.101090.

Mandl, G., ed. 2000. *Tektonik/Strukturgeologische Grundlagen: Erstellung moderner geologischer Karten als Grundlage für karsthydrogeologische Spezialuntersuchungen im Hochschwabgebiet. Unveröffen*. Geologische Bundesanstalt.

Martel, R., P. Castellazzi, E. Gloaguen, L. Trepanier, and J. Garfias. 2018. "ERT, GPR, InSAR, and Tracer Tests to Characterize Karst Aquifer Systems Under Urban Areas: The Case of Quebec City." *Geomorphology* 310: 45–56. https://doi.org/10.1016/j.geomorph.2018.03.003.

Meeks, J., and D. Hunkeler. 2015. "Snowmelt Infiltration and Storage Within a Karstic Environment, Vers Chez le Brandt, Switzerland." *Journal of Hydrology* 529, no. P1: 11–21. https://doi.org/10.1016/j.jhydrol.2015.06.040.

Michot, D., Y. Benderitter, A. Dorigny, B. Nicoullaud, D. King, and A. Tabbagh. 2003. "Spatial and Temporal Monitoring of Soil Water Content With an Irrigated Corn Crop Cover Using Surface Electrical Resistivity Tomography." *Water Resources Research* 39, no. 5: 1138. https://doi.org/10.1029/2002WR001581.

Niggli, P. 1948. *Gesteine und Minerallagerstätten*. Birkhäuser Basel. https://doi.org/10.1007/978-3-0348-7171-6.

Oudin, L., F. Hervieu, C. Michel, et al. 2005. "Which Potential Evapotranspiration Input for a Lumped Rainfall-Runoff Model? Part 2—Towards a Simple and Efficient Potential Evapotranspiration Model for Rainfall-Runoff Modelling." *Journal of Hydrology* 303, no. 1–4: 290–306. https://doi.org/10.1016/j.jhydrol.2004.08.026.

Paterson, W. S. B. 1994. "The Physics of Glaciers." In *The Physics of Glaciers*, edited by W. S. B. Paterson, 3rd ed. Pergamon. https://doi.org/10.1016/B978-0-08-037944-9.50006-6.

Perera-Burgos, J. A., L. G. Alvarado-Izarraras, J. C. Mixteco-Sánchez, et al. 2024. "Hydrogeophysical Evaluation of the Karst Aquifer Near the Western Edge of the Ring of Cenotes, Yucatán Peninsula." *Water* 16: 2021. https://doi.org/10.3390/w16142021.

Perrin, J., P.-Y. Jeannin, and F. Zwahlen. 2003. "Epikarst Storage in a Karst Aquifer: A Conceptual Model Based on Isotopic Data, Milandre Test Site, Switzerland." *Journal of Hydrology* 279, no. 1–4: 106–124. https://doi.org/10.1016/S0022-1694(03)00171-9.

Plan, L. 2016. "Hochschwab." In *Höhlen und Karst in Österreich*, edited by C. Spötl, L. Plan, and E. Christian, 645–660. OÖ-Landesmuseum.

Plan, L., and K. Decker. 2006. "Quantitative Karst Morphology of the Hochschwab Plateau, Eastern Alps, Austria." *Zeitschrift für Geomorphologie*, no. 147: 29–56.

Plan, L., K. Decker, R. Faber, M. Wagreich, and B. Grasemann. 2009. "Karst Morphology and Groundwater Vulnerability of High Alpine Karst Plateaus." *Environmental Geology* 58: 285–297. https://doi.org/10.1007/s00254-008-1605-5.

Plan, L., G. Kuschnig, and H. Stadtler. 2010. "Case Study: Kläffer Spring—The Major Spring of the Vienna Water Supply (Austria)." In *Groundwater Hydrology of Springs*, edited by N. Kresic and Z. Stevanovic, 411–428. Elsevier.

Plan, L., C. Spötl, and G. Bryda. 2019. "Speläologie und Geologie der Hirschgrubenhöhle am Hochschwab (Steiermark)." *Die Höhle* 70: 79–93.

Poulain, A., A. Watlet, O. Kaufmann, et al. 2018. "Assessment of Groundwater Recharge Processes Through Karst Vadose Zone by Cave Percolation Monitoring." *Hydrological Processes* 32, no. 13: 2069–2083. https://doi.org/10.1002/hyp.13138.

Reberski, J. L., J. Terzić, L. D. Maurice, and D. J. Lapworth. 2022. "Emerging Organic Contaminants in Karst Groundwater: A Global Level Assessment." *Journal of Hydrology* 604: 127242. https://doi.org/10.1016/j.jhydrol.2021.127242.

Reisch, C. E., and L. Toran. 2014. "Characterizing Snowmelt Anomalies in Hydrochemographs of a Karst Spring, Cumberland Valley, Pennsylvania (USA): Evidence for Multiple Recharge Pathways." *Environmental Earth Sciences* 72, no. 1: 47–58. https://doi.org/10.1007/s12665-013-2935-5.

Reynold, J. M. 1997. *An Introduction to Applied and Environmental Geophysics*. John Wiley and Sons Ltd.

Ries, F., J. Lange, S. Schmidt, H. Puhlmann, and M. Sauter. 2015. "Recharge Estimation and Soil Moisture Dynamics in a Mediterranean, Semi-Arid Karst Region." *Hydrology and Earth System Sciences* 19, no. 3: 1439–1456. https://doi.org/10.5194/hess-19-1439-2015.

Robert, T., D. Caterina, J. Deceuster, O. Kaufmann, and F. Nguyen. 2012. "A Salt Tracer Test Monitored With Surface Ert to Detect Preferential Flow and Transport Paths in Fractured/Karstified Limestones." *Geophysics* 77, no. 2: B55–B67. https://doi.org/10.1190/geo2011-0313.1.

Sass, O. 2004. "Rock Moisture Fluctuations During Freeze-Thaw Cycles: Preliminary Results From Electrical Resistivity Measurements." *Polar Geography* 28, no. 1: 13–31. https://doi.org/10.1080/789610157.

Şener, A., E. Pekşen, and I. Yolcubal. 2021. "Application of Square Array Configuration and Electrical Resistivity Tomography for Characterization of the Recharge Area of a Karst Aquifer: A Case Study From Menekşe Karst Plateau (Kocaeli, Turkey)." *Journal of Applied Geophysics* 195: 104474. https://doi.org/10.1016/j.jappgeo.2021.104474.

Slater, L., D. Ntarlagiannis, and D. Wishart. 2006. "On the Relationship Between Induced Polarization and Surface Area in Metal-Sand and Clay-Sand Mixtures." *Geophysics* 71, no. 3: A1–A5. https://doi.org/10.1190/1.2187707.

Stevanović, Z. 2019. "Karst Waters in Potable Water Supply: A Global Scale Overview." *Environmental Earth Sciences* 78, no. 23: 1–12. https://doi.org/10.1007/s12665-019-8670-9.

Tague, C., and G. E. Grant. 2009. "Groundwater Dynamics Mediate Low-Flow Response to Global Warming in Snow-Dominated Alpine Regions." *Water Resources Research* 45: W07421. https://doi.org/10.1029/2008WR007179.

Trček, B., M. Veselič, and J. Pezdič. 2006. "The Vulnerability of Karst Springs: A Case Study of the Hubelj Spring (SW Slovenia)." *Environmental Geology* 49, no. 6: 865–874. https://doi.org/10.1007/s00254-006-0182-8.

Uhlemann, S. S., J. P. R. Sorensen, A. R. House, et al. 2016. "Integrated time-lapse geoelectrical imaging of wetland Hydrol Process." *Water Resources Research* 52: 1607–1625. https://doi.org/10.1002/2015WR017932.

Wagner, T., C. Mayaud, R. Benischke, and S. Birk. 2013. "Ein besseres Verständnis des Lurbach-Karstsystems durch ein konzeptionelles Niederschlags-Abfluss-ModellA better understanding of the Lurbach karst system via a conceptional rainfall-runoff model." *Grundwasser* 18, no. 4: 225–235. https://doi.org/10.1007/s00767-013-0234-4.

Ward, S. H. 1990. "Resistivity and Induced Polarization Methods." In *Geotechnical and Environmental Geophysics*, edited by S. H. Ward, 2nd ed., 147–190. Society of Exploration Geophysicists.

Watlet, A., O. Kaufmann, A. Triantafyllou, et al. 2018. "Imaging Groundwater Infiltration Dynamics in the Karst Vadose Zone With Long-Term ERT Monitoring." *Hydrology and Earth System Sciences* 22, no. 2: 1563–1592. https://doi.org/10.5194/hess-22-1563-2018.

Weigand, M., A. Flores Orozco, and A. Kemna. 2017. "Reconstruction Quality of Sip Parameters in Multi-Frequency Complex Resistivity Imaging." *Near Surface Geophysics* 15: 187–199. https://doi.org/10.3997/1873-0604.2016050.

Williams, P. W. 2008. "The Role of the Epikarst in Karst and Cave Hydrogeology: A Review." *International Journal of Speleology* 37, no. 1: 1–10. https://doi.org/10.5038/1827-806X.37.1.1.

Zemann, P. 2024. "Characterization of the Hochschwab Karst Aquifer Flow Regime Using a Water Stable Isotope Approach (Austria)."

Zeydalinejad, N., A. Pour-Beyranvand, H. R. Nassery, and B. Ghazi. 2024. "Evaluating Climate Change Impacts on Snow Cover and Karst Spring Discharge in a Data-Scarce Region: A Case Study of Iran." *Acta Geophysica* 73: 831–854. https://doi.org/10.1007/s11600-024-01400-9.

Zhang, J., C. Sirieix, D. Genty, et al. 2024. "Imaging Hydrological Dynamics in Karst Unsaturated Zones by Time-Lapse Electrical Resistivity Tomography." *Science of the Total Environment* 907: 168037. https://doi.org/10.1016/j.scitotenv.2023.168037.

Supporting Information

Additional supporting information can be found online in the Supporting Information section. **Figure S1.** Overview of volumetric water content (VWC) and temperature sensor installation (modified after Zemann 2024). **Figure S2.** Temporal changes in hydrological parameter during the snowmelt monitoring period expressed in terms of discharge (Q), water electrical conductivity (EC), water temperature (T water). Volumetric water content (VWC) are measured at location 2 at 5 cm depth. **Supplementary Video S1.** Resistivity images converted to a video during the snowmelt monitoring between March 18 and April 8, 2024. The green line indicates the contact of the soil and the bedrock zone and red lines show the contact between the bedrock and the cave zone.